Invited Paper

Scaling diode-pumped Nd^{3+} and Yb^{3+} - doped $YCa_4O(BO_3)_3$ (YCOB) self-frequency doubling lasers

D. A. Hammons*[1], M. Richardson[1,2], B. H. T. Chai[1,3], A. Chin[4] and R. Jollay[4]

[1]CREOL, Univ. of Central Florida Orlando, FL 32816-2700

[2]Laser Energetics Inc. Mercerville, NJ 08619

[3]Crystal Photonics Inc. Orlando, FL 32817

[4]Polaroid Laser Diode Manufacturing and Development, Norwood, MA 02062

ABSTRACT

THE DEVELOPMENT OF DIODE-PUMPED SELF-FREQUENCY DOUBLING (SFD) $YCA_4O(BO_3)_3$ (YCOB) CRYSTALS DOPED WITH ND^{3+} OR YB^{3+} IONS OFFERS AN ATTRACTIVE ALTERNATIVE TO TRADITIONAL INTRA-CAVITY DOUBLING TECHNIQUES USING A SEPARATE NON-LINEAR CRYSTAL. HERE, WE SUMMARIZE THE PROGRESS OF SCALING SFD LASERS TO HIGHER POWERS. MOREOVER, WE EXAMINE THE POTENTIAL AND LIMITATIONS OF THESE DEVICES.

WHILE SFD LASERS ARE POTENTIALLY MORE COMPACT AND LESS COSTLY, SCALING TO HIGHER POWERS IN THE VISIBLE REGION REQUIRES CAREFUL ASSESSMENT OF MODE MATCHING AND CAVITY MODE BRIGHTNESS. COMBINING OPTICAL GAIN AND FREQUENCY CONVERSION IN THE SAME MATERIAL REQUIRES A COMPROMISE BETWEEN THE IDEAL CAVITY MODE FOR MODE MATCHING AND GENERATING THE LARGEST AVAILABLE POWER DENSITY OF THE LASER MODE FOR OPTIMUM FREQUENCY DOUBLING. THE LACK OF ADJUSTMENT OF THE CAVITY MODE INHERENTLY LIMITS SCALING OF SFD LASER OPERATION WHEN USING LOW BRIGHTNESS HIGH POWER LASER DIODES. WE HAVE EMPLOYED A NEW SOURCE DEVELOPED BY POLAROID CORP. USING MULTIPLE HIGH-BRIGHTNESS LASER DIODES TO INVESTIGATE THE POTENTIAL OF INCREASING SFD LASER OUTPUT. WE HAVE THEN COMPARED THE EFFICIENCY OF THIS NOVEL PUMP TECHNIQUE TO A SINGLE DIODE PUMPED SYSTEM TO DETERMINE THE IMPORTANCE OF BRIGHTNESS OF THE PUMP SOURCE TO SFD OPERATION.

Keywords: $YCa_4O(BO_3)_3$, Diode-Pumping, Self-Frequency Doubling, Visible Laser Source

1. INTRODUCTION

Visible continuous wave (cw) laser sources operating efficiently with low cost and having a compact design are of immense interest for many applications. Although cw ion lasers are relatively reliable sources operating at several wavelengths, these devices have a low (<1%) electrical-optical conversion, and require an undesirable large footprint. The foremost coherent light source in the visible region, the diode laser, can now generate powers of a few tenths of a watt of blue emission to a few watts of red emission.[1] However, its poor-spatial quality is inadequate for some applications. Intracavity-doubled, solid-state lasers have satisfied many applications by employing a second, nonlinear optical medium that converts the infrared-laser radiation to the visible. Recent developments in high-power infrared diodes have brought compact diode-pumped versions of these lasers to the market, having high efficiency and long-life expectancy.

We consider a special case of intracavity doubling (ID) known as self-frequency doubling (SFD). This method uses a single crystal both as a nonlinear upconversion medium and as a host for lasing ions such as Nd^{3+} or Yb^{3+}. The laser crystal is itself

* Correspondence: Email: dennis@mail.creol.ucf.edu Telephone: 407 823 3286; Fax: 407 823 6880

In *Laser Diodes and LEDs in Industrial, Measurement, Imaging, and Sensors Applications II; Testing, Packaging, and Reliability of Semiconductor Lasers V*, Burnham, He, Linden, Wang, Editors, Proceedings of SPIE Vol. 3945 (2000) • 0277-786X/00/$15.00

a second-harmonic generator, and when proper temperature- or angle-tuned phase-matching conditions are met, a portion of the circulating laser-power is converted to twice its frequency. Thus, we obtain intracavity frequency doubling without the insertion of a secondary, nonlinear-optical medium. Relative to ID using two crystals, a SFD laser has advantages in that it incorporates lower reflection, absorption and scattering losses and allows a simpler and more robust resonator design. While these are desirable features, unfortunately very few crystals possess the unique combination of optical and physical properties necessary for successful SFD operation.

The recent increased interest in SFD lasers has been primarily driven by the development of a new family of nonlinear optical crystals, the rare-earth calcium oxyborates, $ReCa_4O(BO_3)_3$ (ReCOB).[2] Advances in this new family of optical materials have primarily been in two particular crystals $YCa_4O(BO_3)_3$ (YCOB) and $GdCa_4O(BO_3)_3$ (GdCOB). Many recent papers have described these materials and their SFD lasing properties when doped with either Nd^{3+} or Yb^{3+} ions.[3-8] SFD laser action was first demonstrated by Johnson *et al.*[9], with Tm-doped $LiNbO_3$. SFD laser operation using Nd^{3+}:MgO:$LiNbO_3$[10,11] was later reported, but was thwarted by poor optical quality and the occurrence of photorefractive damage in the crystal.[9-11] A more promising SFD crystal, Nd^{3+}:$YAl_3(BO_3)_4$ (NYAB), was discovered at about the same time period by two groups Dorozhkin *et al.*[12] and Lu *et al.*[13]. NYAB has a large nonlinear coefficient, high emission cross-section and high damage thresholds.[14,15] This material has been operated as a free running and a Q-switched system with flashlamp[16] (including Cr^{3+} sensitization[17]) and diode-laser pumping.[14,18] The three strongest emission lines have been self-doubled.[14,19-21] NYAB has low concentration quenching rates allowing for high concentrations of Nd ions. Therefore, in a sample with a Nd concentration of 10%, the metastable-state lifetime is 60 μs and the 1.06 μm laser line has an emission cross section[22] of 2×10^{-19} cm^2 and a linewidth of 30 cm^{-1}. The luminescence quantum efficiency[22] is about 15%. The nonlinear optical coefficient of the host material is almost four times that of KH_2PO_4 crystals. However, this crystal suffers from poor optical quality, low production yield and self-absorption at 530 nm.[2,13] The recent interest in SFD laser operation has now prompted the investigation of other hosts and the use of Yb^{3+} as a lasing ion in other nonlinear materials.[23-26]

In this paper, we review the physical and optical properties of the laser host YCOB. Lasers based on this host material will open new opportunities for the development of compact, high-power, frequency-agile visible and near IR laser sources for ultrashort pulses. Efficient diode-pumped laser action with both Nd-doped and Yb-doped YCOB has been demonstrated.[4,27] Moreover, SFD operation has been demonstrated with the potential for scaling this material to higher SFD powers. Scaling is performed using a novel high-power diode system as the pump source.

2. PHYSICAL AND OPTICAL PROPERTIES OF YCOB

All the experimental samples used in the measurements reported here were grown by the Czochralski method from melts contained in iridium crucibles. ReCOB compounds have a congruent melting nature; thus, large single-crystals with high optical quality can be economically grown.[2,28] The starting composition melts at 1510 °C and is grown with a rotation rate of 15-20 rpm and pulled at 1–1.5 mm/h in a neutral atmosphere.[28] Boules, 75 mm in diameter and 200 mm long, are commercially available.[2,28] The large size also allows for large-aperture nonlinear crystals for high-power lasers. All the samples were either grown at the Crystal Growth Laboratory, CREOL, University of Central Florida, or by Crystal Photonics Inc.

The ReCOB structure was first reported[29] in 1989 as a new compound calcium fluoroborate, $Ca_5(BO_3)_3F$, and it was assigned to the curium (Cm) space group, whose elements are monoclinic and asymmetric. The actual work on calcium rare-earth oxyborate compounds was first reported in 1991 by Khameganova *et al.*[30]. It was obtained serendipitously from PbO flux, during the preparation of $Ca_3Sm_2(BO_3)_4$. In 1992, Norrestam *et al.*[31] synthesized through high-temperature solid-state reactions a number of rare-earth analogues of Re calcium oxyborates, $ReCa_4O(BO_3)_3$ where Re = La^{3+}, Lu^{3+}, Y^{3+}, Sm^{3+}, Gd^{3+}, Er^{3+}, or Nd^{3+}. They suggested the potential of these crystals as laser materials, but their crystals were too small to demonstrate laser action. Moreover, they showed that these compounds melt congruently making these materials more plausible for obtaining large single crystals by the Czochralski pulling method. In 1993, researchers from Russia essentially completed the whole series by synthesising[32] $ReCa_4(BO_3)_3O$ with Re = Lu^{3+}, Tb^{3+}, and Gd^{3+}. Further studies have shown that for both large ions, such as lanthanum and for small ions, such as lutetium, the crystalline structure is less stable and no longer congruent,[2] Thus the most stable sizes are between gadolinium and erbium, where the melt is also congruent.[2] The first large size GdCOB crystals were reported by Aka *et al.* in 1996.[33] They demonstrated single crystals of GdCOB about 70 mm long and 20–30 mm in diameter grown by slowly pulling boules from a molten charge, which consisted of sintered prereacted powder. They also reported the linear and nonlinear optical characteristics of GdCOB and its potential as a self-frequency doubling laser material with Nd^{3+} doping.[3] A year later, Iwai *et al.* reported the growth and optical characteristics of GdCOB and

YCOB,[34] as well the observation of SHG. A number of reports has since followed demonstrating SHG and SFD for both YCOB[4,6,7,35-36] and GdCOB.[3,5,8,37-39]

Some confusion surrounds the description of crystals with low-symmetric, monoclinic systems like YCOB. For crystals with high symmetry such as cubic, tetragonal, etc., both the optical indicatrix axes X, Y, Z and the intrinsic crystallographic axes a, b, c of the crystal are collinear. In the monoclinic system, only the b-axis is collinear with the Y-axis. The non-orthogonal a- and c-axes are coplanar but positioned at certain angles with respect to X- and Z- axes. In our work, we use an orientation according to Figure 2.1 for the spectroscopic and laser samples. Reference 28 provides more details regarding the procedure for this orientation.

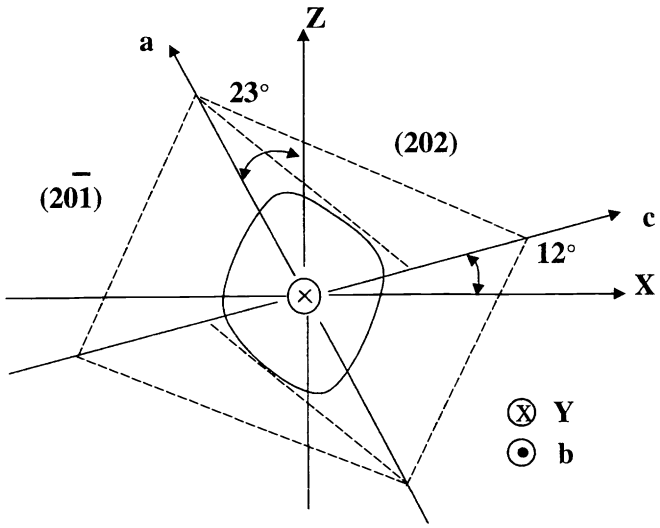

Figure 2.1. Orientation[28] of the X, Y, and Z optical indicatrix axes relative to the a, b, and c crystallographic axes of $YCa_4O(BO_3)_3$

2.1 Physical properties of YCOB

To withstand the severe operating conditions of practical lasers, solid-state host materials must have good mechanical, thermal and chemical properties. The desirable properties include hardness, chemical inertness, absence of internal strain and refractive index variation, resistance to radiation-induced color centers and ease of fabrication.[40] Such physical properties of the host material often determine the maximum power capabilities of a laser system. Table 2.1 presents the physical properties determined for the host structure YCOB compared to several other oxide and fluoride laser and nonlinear crystalline hosts.

Property	YCOB[28]	SVAP[41]	YLF[40,42]	YAG[40]	KD*P[43]	LBO[43,44]	KTP[43-45]
Thermal conductivity κ (W/mK)	2.60 (a) 2.33 (b) 3.01 (c)	1.9 (a) 2.0 (c)	7.2 (a) 5.8 (c)	10	1.9 (a) 2.1 (c)	3.5	2.0 (X) 3.0(Y) 3.3(Z)
Thermal Expansion α (x 10^{-6}/K)	8.39 (a) 5.18 (b) 9.17 (c)	7.7 (a) 10 (c)	13 (a) 8 (c)	6.7	19 (a) 44 (c)	108 (X) -88 (Y) 34 (Z)	11 (X) 9 (Y) 0.6 (Z)
Thermal-optic coefficients (x 10^{-6}/K)	2.0 (X)[a] 2.5 (Y)[a] 1.2 (Z)[a]	-8 (a)[b] -10 (c)	-4.3 (a) -2 (c)	8.9	-31 (o) -21 (e)	-1.8 (X) -13.6 (Y) -8.4 (Z)	11 (X) 13 (Y) 16 (Z)
Fracture Toughness[c] K_c (MPa$\sqrt{m}$)	-	0.36	1.4	2.7	-	-	-
Hardness	6.0~6.5	413	260-325	1320-1380	-	6	~5
Hydroscopic susceptibility	None	None	None	None	High	Low	None

Table 2.1. Physical properties of laser host and nonlinear crystal

2.2 Optical and spectroscopic properties of Nd^{3+}:YCOB

The absorption and spontaneous emission spectra of Nd-doped YCOB illustrate many of the reasons for its attractiveness as a medium for diode-pumped SFD lasers. Because of the interest in making a laser-pumped laser using this material, Figure 2.2 presents the orientationally resolved absorption spectra of Nd^{3+}:YCOB for the ranges that are of interest for AlGaAs laser

diode-pumping. The strongest absorption for diode pumping occurs for light polarized along the Z-axis with the two peaks at 794 nm and 812 nm. The optical behavior of Nd^{3+} ions in this low site-symmetry varies as the optical propagation-direction is rotated from the X-axis to the Y-axis.[46] The absorption coefficient varies with angle and has been measured to be 2.9 cm^{-1} at 28° and 3.8 cm^{-1} at 35° from the X-axis for SFD laser-operation in the red at 666 nm and in the green at 530 nm.[4,6] We also see that the absorption coefficient for the second harmonic of 1060 nm in the polarization perpendicular to the lasing polarization is 0.46 cm^{-1}. For approximately the same doping percentage, this is approximately half the absorption coefficient for NYAB[14] at 531 nm of 0.94 cm^{-1}.

The spontaneous emission spectra of Nd^{3+}:YCOB is shown in Figure 2.3. The polarized emission spectrum indicates several peaks corresponding to the three common transitions of Nd^{3+} active ions. The strongest emission of the $^4F_{3/2} \rightarrow {}^4I_{11/2}$ transition is at 1060 nm for the polarization parallel to the Z-axis. This wavelength can be frequency-doubled to 530 nm to generate green light. The strongest emission of the $^4F_{3/2} \rightarrow {}^4I_{13/2}$ transition is at 1332 nm, also polarized parallel to the Z-axis. By cutting along the phase-matching direction at this wavelength, the 1332 nm fundamental emission can be self-frequency doubled to generate the red light at 666 nm.[6]

The emission corresponding to the transition of the $^4F_{3/2} \rightarrow {}^4I_{9/2}$ is much weaker compared to the 1.06 and 1.3 μm. It has several peaks, with the sharpest one polarized parallel to the Y-axis at 936 nm. If laser action can be achieved at 936 nm, frequency doubling would generate blue light at 468 nm. In addition, self-sum-frequency mixing of the 1060 nm and the 812 nm pumping can be used to create blue emission at 458 nm .Thus, in principle, it is possible to achieve RGB three colors through self-frequency doubling.

The radiative fluorescence lifetime of the excited $^4F_{3/2}$ J manifold in Nd^{3+}:YCOB at room temperature was measured for 5% of Nd_2O_3 placed in the melt. Using both powder and optically-thin polished samples, the fluorescence lifetime was measured using a birefringently-tuned Q-switched Cr:$LiSAlF_6$ laser to excite the samples at 812 nm. The lifetime was found to be 100 μs with a single exponential-decay.

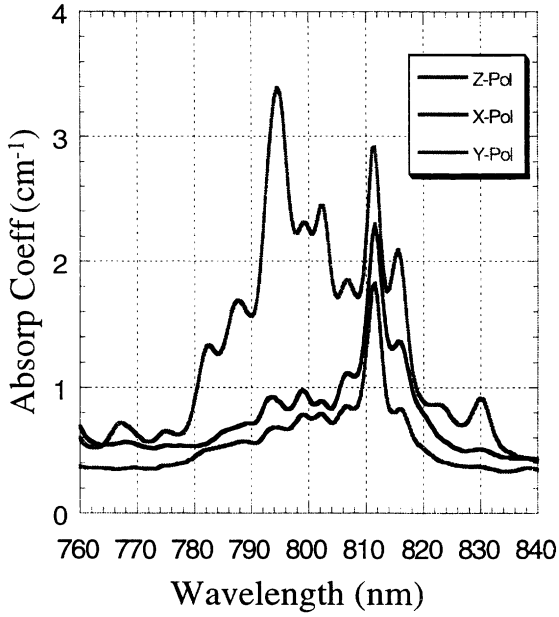

Figure 2.2. Absorption spectra of Nd^{3+}:YCOB[4]

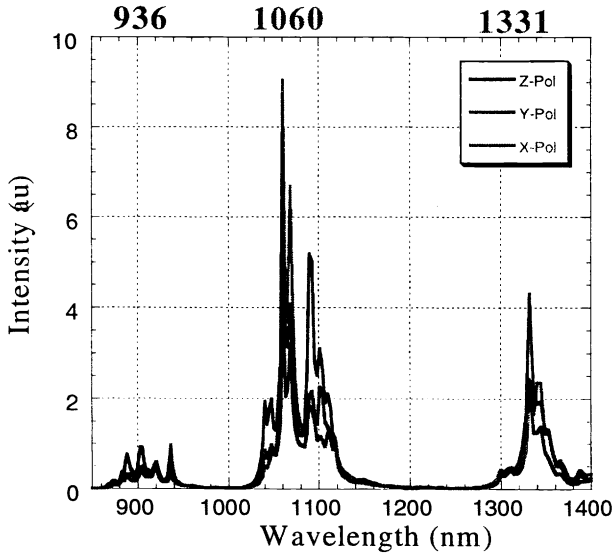

Figure 2.3. Spontaneous emission spectra of Nd^{3+}:YCOB[4]

We have examined the spectroscopic properties of Yb^{3+} in YCOB for prospective laser operation. As with other Yb^{3+}-doped gain media, laser action is based on the one excited 4f manifold, approximately 10,000 cm^{-1} above the ground state.[47] The large vibronic components of the $^2F_{7/2} - {}^2F_{5/2}$ transition gives rise to a broad absorption feature at 900 nm and an additional absorption line at 976 nm. The absorption and emission spectra are shown in Figure. 2.4. and 2.5, respectively, for light polarized parallel to the X, Y, and Z axes. The fluorescence spectrum shows multiple emission lines from 950 nm to 1090 nm with the strongest emission feature at 1030 nm. Using a Q-switched Cr:$LiSAF_6$ laser operating at 900 nm, the fluorescence decay time was measured to be approximately 3 ms for a 20% doped thin-sample, which is considerably longer than other oxide crystals.

The absorption spectra shows that as a laser medium, Yb^{3+}:YCOB can be optically pumped using diode lasers at 900 nm or 977 nm. Pumping the broad absorption-band at 900 nm allows the wavelength of the laser diode to drift, placing less constraint on the temperature control of the laser diode. However, diodes at this wavelength are less advanced and are not widely available. High-brightness laser diodes operating at 980 nm are available as a consequence of their use in telecommunication industry providing for reduced cost and a more reliable pump source. In addition, the Stark shift is reduced, which increases the laser efficiency and lowers the amount of heat produced as a result of non-radiative relaxation. The disadvantages of this pumping technique lie in the stringent control of the diode wavelength and the optical coating for the pump mirror that is needed. At this point, with improved coating technology forthcoming, the advantages of 980-nm longitudinal diode pumping will outweigh its disadvantages.

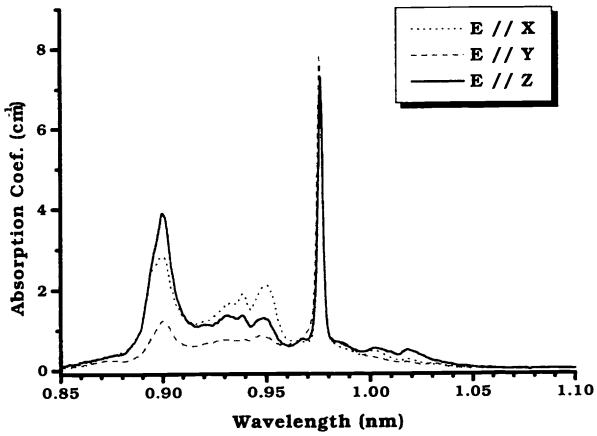

Figure 2.4. Absorption spectra of Yb^{3+}:YCOB[7]

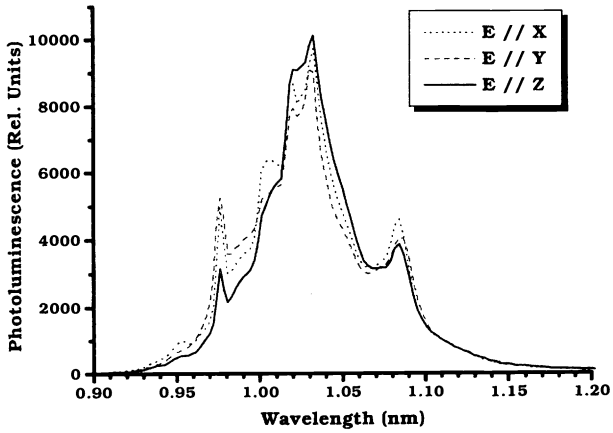

Figure 2.5. Spontaneous emission spectrum of Yb^{3+}:YCOB[7]

3. LASER ACTION AND SFD OPERATION IN YCOB

3.1 Laser action and SFD operation of Nd^{3+}:YCOB

Our diode-pumped experiments have been performed with a simple, 10 cm long, laser resonator, which is longitudinally pumped. A high-brightness, AlGaAs laser-diode (Polaroid POL-5100BW) with a maximum output power of 1.85 W from a 100 μm stripe centered at a 812 nm was used. A 125-μm diameter fiber-lens was utilized to collect the emission from the laser diode's fast axis and helped equalize the divergence from the fast and slow axes. After the micro lens, a 50-mm focal-length achromatic-doublet lens was used to collect the diverging pump beam. With the light collimated, the pump beam was refocused with a 60 mm focal length Gradium™ plano /convex lens to a ~50x70 μm (FWHM) spot size, as measured with a scanning slit beam profiler. The hemispherical laser resonator consisted of a highly reflective rear mirror and a 10-cm radius of curvature output coupler. The 3x3x5 mm long, 5% Nd^{3+}:YCOB crystal was placed next to the high reflector. The crystal was experimentally examined using a Nd:YAG laser to determine the optimum angle for Type I critical phase-matching in the XY plane, 90° from the Z-axis at 1064 nm. Based on the Sellmeier equations of Mougel *et al.*[48], the crystals were cut with the polished faces aligned at an angle of 34.97° from the X-axis. Both surfaces were coated with a triple band anti-reflection coating which had less than 1% reflectivity at 1060, 530 and 812 nm. The crystal absorbed approximately 75% of the incident pump light

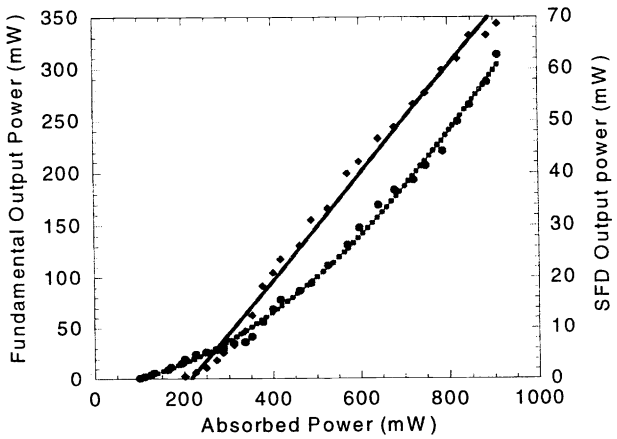

Figure 3.1. Fundamental and SFD output power of Nd^{3+}:YCOB[4]

at full current to the diode. The pump laser polarization was parallel to the Z-axis and was focused into the crystal through the rear mirror, which was 95% transparent at 812 nm. The fundamental (1060 nm) output power versus the absorbed pump power is shown in Figure 3.1 for 2% transmission output coupling. The polarization of the laser output was parallel to the Z-axis. Output powers exceeding 340 mW for 900 mW of absorbed pump power were obtained with a slope efficiency of 51%.

Efficient diode-pumped self-frequency doubling at 530 nm was demonstrated utilizing the same crystal. The resonator design was identical to that described above. To maximize the SFD output, the output coupler was a 10 cm ROC mirror, highly reflective at 1060 nm (R=99.82%) and highly transmissive (T>96%) at 530 nm. The phase matching was optimized by adjusting the crystal angle, and mode size by adjusting the cavity length. The SFD power as a function of absorbed pump power is also shown in Figure 3.1. Over 62 mW of 530 nm laser light was obtained with 900 mW of pump power absorbed in the crystal. At this power, the spatial mode profile of the SFD laser output as measured by a Spiricon LBA-100A was multi-mode. The onset of SFD output occurred for only 100 mW of diode power absorbed in the crystal. The spectrum of the SFD output consisted of a single, narrow (<0.6 nm) line at 530.3 nm.

SFD was also observed at 666 nm, with a similar laser configuration and a 4 x 4 x 6 mm crystal cut for Type I phase matching with a phase-matching angle of 27° to the Y axis[6]. The 812 nm diode pump threshold power for red SFD laser action was 270 mW, with peak powers of 16 mW being obtained for pump powers of 950 mW[6]. SFD laser action on one of the $^4F_{3/2} \rightarrow {}^4I_{9/2}$ transitions in the region of 940 nm is far more difficult to demonstrate. Lasers based on these transitions are inherently quasi-three-level systems and therefore require higher pump powers. Although our attempts to observe lasing at this wavelength were unsuccessful[6], our experiments were not well optimized, and we anticipate that laser action at 936 nm, and possibly SFD operation at 468 nm will eventually be demonstrated.

3.2 Laser action and SFD Operation of Yb^{3+}:YCOB

Our interest in Yb doped YCOB stems from its broad emission band characteristics, as well as its nonlinear optical properties. Ytterbium-ion doped solid-state lasers have received considerable attention because their favorable spectroscopic properties could lead to compact high average power diode pumped laser systems emitting either tunable or ultrashort infrared radiation. Laser action has been demonstrated in a number of Yb^{3+}-doped crystals such as YAG,[49,50] S-FAP[51] and glasses[52] We have investigated Yb^{3+}:YCOB as a laser material in cw operation under Ti:Sapphire and laser-diode pumping. A 10% and 20% doped Yb^{3+}:YCOB laser rod, mounted on a thermoelectric cooler with a cross-section of 5 mm x 5 mm, a length of 13 mm, was cut with the x-axis collinear with the laser axis. The uncoated Yb^{3+}:YCOB crystal was placed next to the high reflector in a cavity design as described above. The pump beam was focused with a 8.8-cm focal length plano/convex lens to a ~70 μm (FWHM) spot size as measured with a scanning slit beam profiler. The crystal absorbed more than 90% of the incident pump light. Figure 3.2 shows the observed cw oscillator output power as a function of absorbed pump power under Ti:Sapphire pumping. Using a 1% transmitting output coupler, slope efficiencies of 29% and 36% were achieved for the 10% and 20% doped crystals, respectively[7]. The threshold of the absorbed pump power for lasing was high with 230 mW and 370 mW for the two samples. In both cases, the laser emission was weakly polarized. Unexpectedly, laser action was observed at longer wavelengths than the peak of the fluorescence emission (~ 1030 nm) for both the 10% and 20% doped media at 1050 nm and 1090 nm, respectively. We attribute this to a consequence of self-absorption on the short-wavelength side of the emission band. Most

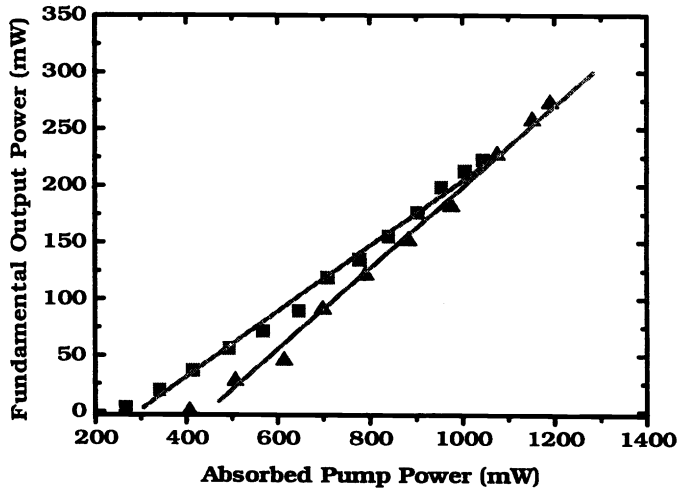

Figure. 3.2. Laser output power at 1050 nm for 10% doped Yb^{3+}:YCOB (Squares) and laser output power at 1085 nm for a 20% doped Yb^{3+}:YCOB (Triangles) as a function of absorbed 900 nm pump power[7].

probably careful selection of crystal dopant concentration and length will allow laser action across the whole emission band, and the achievement of higher slope efficiencies.

Experiments demonstrating diode-pumped operation were performed using either a 905 or 977 nm diode laser. The hemispherical laser resonator consisted of a flat, highly reflective rear mirror and a 10-cm radius of curvature output coupler (OC) as discussed earlier. The 20% Yb^{3+}:YCOB laser rod, mounted on a thermoelectric cooler had a cross-section of 2 mm x 6 mm, a length of 3 mm, and was cut with the x-axis collinear with the laser axis. The temperature of the crystal was maintained at room temperature (23 °C) with the TE cooler. The pump laser polarization was parallel to the Z-axis and was focused into the crystal through the rear mirror. The rear mirror developed by Quality Thin Films, was highly reflecting from 1040 - 1150 nm and over 95% transparent at 977 nm. The diode-pumped output power versus the absorbed pump power with a 2% OC is shown in Figure 3.3 for 1050 nm and 1041 nm wavlengths for 905 and 977 nm pumping, respectively. Slope efficiencies of 27% and 40% were obtained showing improved operation due to a smaller Stokes shift for 977-nm diode-pumping. Operation using both laser-diode pump wavelengths has shown operation from 1030 to 1095 nm. The reduced reflectivity of the pump mirror at wavelengths below 1040 nm limits the available range.

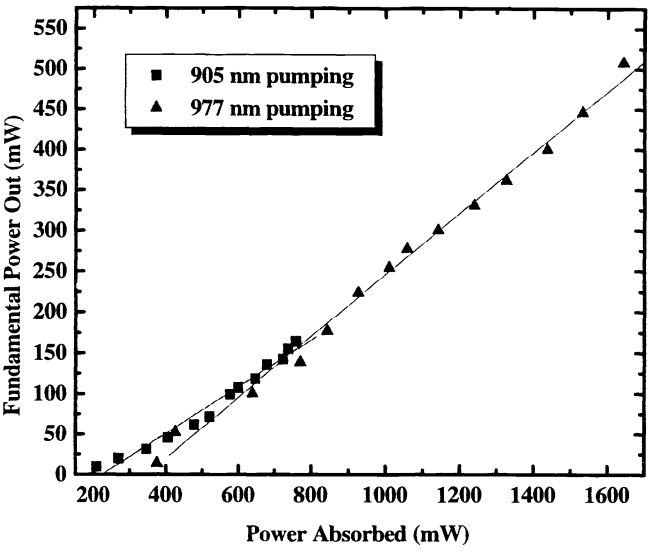

Figure 3.3. Laser output power at 1050 nm for 905 nm diode-pump power absorbed (Squares) and laser output power at 1041 nm for 977 nm diode-pump power absorbed (Triangles) for a 20% doped Yb^{3+}:YCOB crystal.

We have also observed self-frequency doubling in Yb^{3+}:YCOB under cw diode-pumping. The 20% Yb^{3+}:YCOB crystal used for this test was cut based on the Sellmeir equations of Mougel *et al.*[48], with the crystal's X-axis at 34.97° to the laser axis. In order to obtain SFD operation, the intracavity power density was increased by changing the output coupler to a 10-cm ROC mirror with high reflectivity at 1050 nm (R > 99.7%) and high transmission (T > 96%) at 530 nm. SFD operation was found to occur from 520 to 547 nm. However, less than 1 mW of visible laser light was obtained with the maximum pump power absorbed in the crystal. The SFD efficiency was low due to the laser bandwidth being larger than the angular acceptance bandwidth for phase-matching (1.3 mrad-cm). It would improve significantly with the use of a frequency selective element in the cavity to narrow the linewidth of the fundamental emission.

4. SCALING SFD OPERATION: POTENTIAL AND LIMITATIONS

4.1 Scaled laser action and SFD operation in Nd^{3+}:YCOB

A number of techniques have been devised to scale the overall pump-power of end-pumped solid state lasers. These include the use of polarization combination, high power diode bars, multiple sources using fiber bundles,[53,54] light funnels[55] or multiple entrances to many gain elements.[56] Angular multiplexing of diode bars has been effectively used to analyze scaling limits of diode-end-pumped Nd:YAG lasers[57]. Here, we demonstrate a novel technique for combining in free space, the light from three separate multi-mode laser-diodes for improved pump-power density. Angular-multiplexing individual high-brightness laser-diodes was first described by Fan *et al.*[58,59]. They used three diode-lasers closely packed in the plane perpendicular to the junction and a combination of cylindrical lenses to collimate and focus the light.[58] The high-brightness multi-laser source, developed by Polaroid Corp.,[60] similarly places the near-field images of up to eight separate multi-mode diode-lasers side-by-side on a multi-faceted mirror, which redirects the beams so they are juxtaposed and parallel.[60] The diode-laser packages (illuminators) are arranged roughly on a circle with the plane parallel to the junction placed perpendicular to the optical axis. Each illuminator consists of a 100-μm strip-width diode-laser, a microlens and anamorphic

optics. The mirror is monolithic with eight diamond-turned facets, each having a projected width in the output direction of 300-μm giving a full projected width of 2.4 mm.[60]

The advantages of using this configuration, compared monolithic diode bars are in the individual controls over their wavelength and their polarization. Separate temperature control of each laser-diode permits its spectrum to be tightly matched to a narrow absorption-peak (< 0.8 nm FWHM). In addition, the overall output from the high-brightness source can be linearly polarized.

Additional optics was placed on the output of the multi-diode high-brightness source to reduce the output spot-size and focus the light into the crystal. The output from three diode-lasers was reduced using a spherical-telescope and then focused using a 50 cm focal-length lens to a pump mode spot-size of ~ 170 x 220 μm (FWHM). The three laser-beams were found not to be completely parallel, thus adding loss to the pumping geometry. This effect was also seen in attempts with larger-ratio beam-reducers, which resulted in larger pump-mode spot-sizes because the individual beams were diverging from each other. The principal loss in brightness occurs because the mirror facets are 300 μm wide and the near-field images formed on them are only 50 μm, giving an inherent 6:1 loss.[60] Smaller facets and tighter tolerances on the alignment to increase parallelism would increase the brightness of the source.

The laser resonator consisted of a flat pump input-mirror M_1 and a concave output-mirror M_2. The pump-laser polarization was parallel to the Z-axis and focused into the crystal through the rear mirror, which was 96% transparent at 812 nm. The reflectivity of M_1 was R > 99.9% for both the fundamental and the second-harmonic wavelengths. Three different output-coupling mirrors, M_2, were used for operating the laser in either the fundamental or SFD modes of operation. The mirrors used were highly reflecting or had an output coupling of 1% or 2% at 1060 nm with a 10-cm radius of curvature. The highly reflecting mirror was also coated to be highly transmissive at 530 nm (T > 94%). The laser cavity was near hemispherical and was operated close to the limit of optical stability. The laser crystal was mounted between to copper blocks. Each block was temperature controlled using thermoelectric coolers, which were heat-sunk to two water-cooled aluminum-blocks. The laser-crystal holder was secured to a two-axis rotational-adjustment kinematic mount.

The Nd^{3+}:YCOB crystal was pumped with up to three diode-lasers using this multi-laser high-brightness source. A schematic of the end-pumped SFD Nd^{3+}:YCOB laser is shown in Figure 4.1. The surfaces of the pump optics were not AR-coated for the pump wavelength. Thus, the transmission of the pump optics was only 90% at 812 nm. The focus of the pump beam was located on the front facet of the Nd^{3+}:YCOB crystal, which was placed next to the flat high-reflector.

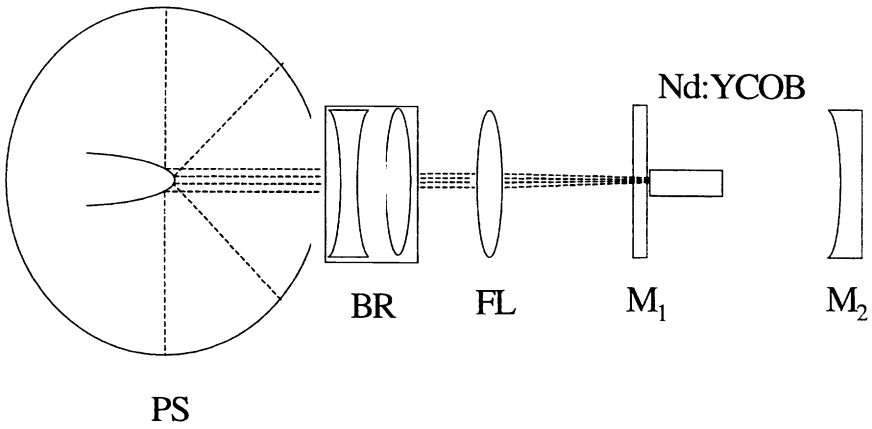

Figure 4.1. Schematic of the end-pumped high-power SFD Nd^{3+}:$YCa_4O(BO_3)_3$ laser system.
PS: pump source, BR: beam reducer, FL: focusing lens, M_1: pump input mirror, M_2: output mirror

Fundamental laser-operation is shown in Figure 4.2. The cw laser-output was characterized using from 1 to 3 diode laser pump-sources. The highest slope efficiency of 51.8% was observed with a 2% output coupler. The fundamental output power exceeded 1.3 W for 3.4 W of absorbed pump power. An increase in the threshold as more than one diode laser was activated indicates that not all the diode lasers were pumping the same cavity mode volume.[58] Thus, the pump mode-volume was increasing, which reduces the pump beam-brightness. The scaling of the SFD output with the number of diode lasers was also investigated. Figure 4.3 shows SFD laser operation of Nd^{3+}:YCOB for 1 and 3 diode-laser pump-sources. At the maximum pump-power of 3.4 W, the laser generated more than 85 mW of visible 530-nm radiation.

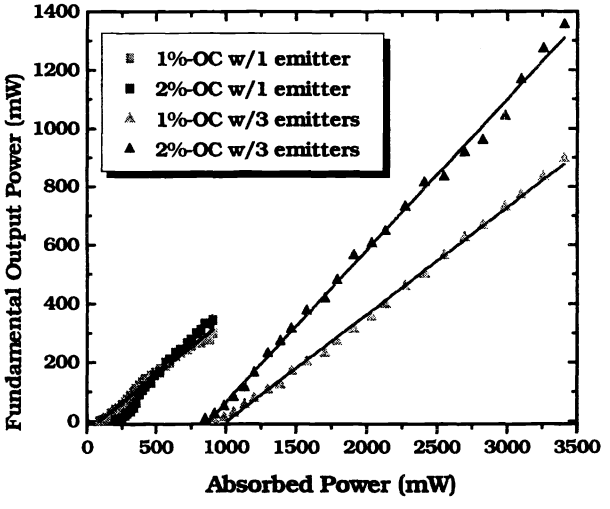

Figure 4.2. Fundamental laser output at 1060 nm using 1 and 2% output coupling. Pumping is by one, ■, or three, ▲, laser-diodes.

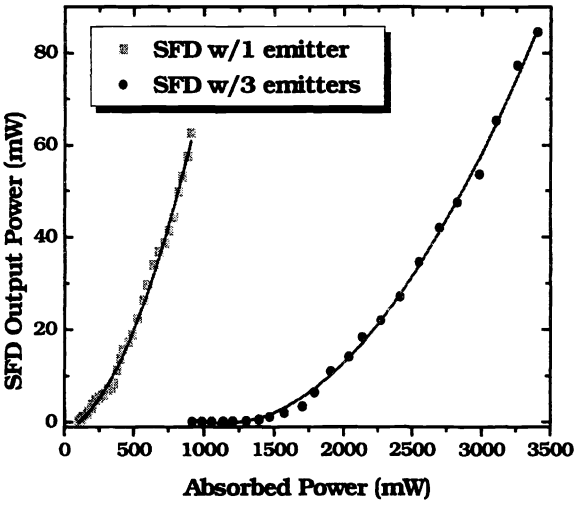

Figure 4.3. Self-frequency doubled laser output at 530 nm. Pumping is by one, ■, or three, ▲, laser-diodes.

The beam-quality parameters for the SHG and fundamental operation were measured with a scanning slit beam-profiler. The beam-quality measurement was obtained by generating a beam waist using a lens.[61] For the second harmonic, M^2= 6.2 and 5.3 for the parallel and perpendicular planes to the optical axis. The fundamental laser-output had a beam-quality measurement of M^2= 3.6 and 1.9 for the parallel and perpendicular planes to the optical axis.

As with most intracavity frequency-doubled lasers with many oscillating longitudinal modes, the SFD process in Nd^{3+}:YCOB has large amplitude fluctuations due to longitudinal-mode coupling through the sum-frequency generation process, which strongly modulates the second-harmonic light.[62] This noise can be shown either as a typical oscilloscope trace in time, or as a noise percentage integrated over bandwidth. A measure of the highest power spike and lowest power spike can give large deviations in the peak-to-peak noise level. Here, we have measured the amplitude stability in terms of the spectral density of the relative-intensity noise (RIN).[63,64] The RIN was measured by detecting the 530 nm light using a silicon photodiode and a spectrum analyzer. The relationship between RIN expressed in dB/Hertz and the root-mean-square (RMS) noise is:[64]

$$RMS = \sqrt{\int_{f_{min}}^{f_{max}} RIN(f)df} \tag{4.1}$$

where f_{min} and f_{max} are the range of the RMS noise bandwidth. Here, we have determined the RMS noise to be 3.1% for the case of maximum green emission. This is worse than the previously published measurement of 8% peak-to-peak noise

fluctuation[4] since in practice the peak-to-peak noise is 4 times the RMS noise.[64] Other SFD lasers have had between 3% and 6% peak-to-peak amplitude fluctuation.[65] This RMS-noise fluctuation is a consequence of not only multi-longitudinal mode oscillations but also coupled polarization-modes[66] and feedback instabilities on the laser-diode source due to the absence of anti-reflection coatings on the pump optics. There are several methods of suppressing the chaotic instabilities and noise associated with green lasers.[67-69] However, in these experiments no attempts were made to reduce the RMS noise of the SFD output. Future cavity designs will include measures to limit amplitude fluctuations.

4.2 Scaling SFD operation: Limitations

While integrated systems are often more advantageous, SFD crystals are not without their limitations. One of the major problems with SFD in Nd – doped materials is the strong absorption at the wavelength of the doubled light. This effect is so strong in NYAB that design considerations must take into account the absorption coefficient at the second harmonic.[14] The lower absorption at the second harmonic in Nd^{3+}:YCOB is an important attribute. Another problem is the temperature-dependent change in the phase-matching condition that occurs due to the heat generated in the optical pumping. Because of the phase-matching requirements for the primary- and secondary-harmonic wave in a nonlinear crystal, efficient SFD laser crystals are very sensitive to crystal orientation alignment, optical path length, and temperature. To compensate for crystal orientation and alignment, Yoshimura *et al.*[37] have found that non-critical phase-matching is achievable by varying the ratio of yttrium and gadolinium in GdYCOB ($Gd_xY_{1-x}Ca_4O(BO_3)_3$). Thus, more stable operation will be obtainable at the higher pump powers. The one major drawback left is cavity mode control for both pump mode overlap and efficient harmonic conversion.

Our comparisons between Ti:Sapphire-pumping and single diode-pumping, indicated that the brightness characteristics of diodes have a crucial influence in the second-harmonic output. The lower absorption cross-section of Nd^{3+}:YCOB (as compared to NYAB) requires a higher-brightness pump-source to obtain the same laser operation as described by Fan *et al.*[70]. Moreover, low cost, low-brightness high-power diodes require a larger cavity-mode to overlap well with the pump mode for efficient laser operation. For a given pump power, the larger cavity-mode decreases the intracavity fundamental-intensity, thus lowering the conversion efficiency to the second harmonic. The pump focusing geometry and the configuration of the laser cavity have thus to be a compromise between the focusing required for optimum laser performance and the waist size of the TEM_{00} mode, which provides optimum frequency-conversion. By multiplying the laser slope efficiency described by the spatial-mode overlap between the cavity mode and the pump mode with the second-harmonic output, we can obtain a plot describing the optimum cavity-mode control for conversion of the pump radiation into frequency-doubled laser light. Using reported models for diode pumping,[71-74] Figure 4.4 shows the resulting change in converted photons as a function of the ratio of the two modes (pump mode/cavity mode). While diode-pumping of Nd^{3+}:YCOB for strictly laser operation would be much more efficient for a mode ratio of less than one, the harmonic conversion is greatly reduced for the larger cavity mode. We see from the plot of the SFD conversion efficiency that optimal operation would occur for ratios greater than 2 but less than 2.5.

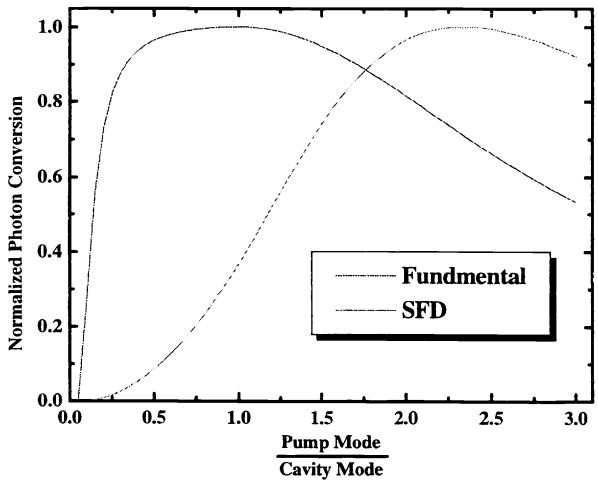

Figure 4.4 Normalized photon-conversion as a function of the pump to cavity mode ratio for fundamental output and for SFD output.

The optical pumping process of all solid-state lasers generates some amount of localized heating of the laser material. Heating results from several causes: quantum defect, quenching mechanisms, thermalized terminal laser level(s), and absorption of the pump photons by the host material.[40] In the limit, the combination of volumetric heating and surface cooling can result in thermo-mechanical failure from stress, which occurs when the induced temperature gradients in the laser material exceed the tensile strength of the material. To first order, one can infer a material's intrinsic thermo-elastic strength from its thermal conductivity. As a nonlinear crystal, the thermal conductivity of YCOB is better than KDP and BBO and

comparable to KTP. However as a laser medium, its thermal conductivity is about half that of YVO_4 and one-fourth that of YAG. Thus, ReCOB is a weak material for scaling to very high laser powers.

Stress fracture of the laser crystal is the ultimate limit to increasing its thermal load, and the laser output power. The maximum absorbed thermal-power per unit length by a laser rod for a slab geometry is:[75,76]

$$\frac{P_a}{l} = 12 \cdot R_T \cdot \frac{w}{t} \tag{4.2}$$

where w/t is the aspect ratio of width to thickness and R_T is a thermal stress-resistance figure of merit (FOM) for the material. The FOM is valid for a given flaw-size and is dependent on the intrinsic material-properties.[40,76] In some experiments of thermal stress fracture, we measured the power absorbed per unit length to determine the value R_T in Nd^{3+}:YCOB. We began by measuring the power incident on the crystal. Using the well-known Beer's law,[40] we calculated the power absorbed over the length of the crystal up to the point where subsurface cracking occurred.

In three experiments, the initial input power on the front face of the crystal was measured to be 13.5, 12.3 and 10.9 W with the associated fracture occurring at 0.23, 0.62, and 0.93 mm beyond the input face, respectively. Although these measurements are fracture-size dependent, all three propagated cracks ranged from 50 to 100 μm in width. Table 4.1 gives the associated power absorbed per unit length and a calculated thermal stress-resistance figure-of-merit. The estimated FOM is better than $YLiF_4$ and comparable to silicate glass.[77] Using the measured thermal-conductivity and thermal-expansion values with reasonable estimates for the elastic modulus, Poisson's ratio and the tensile fracture strength, we see that the thermal stress FOM is 1.5 to 2 times the experimentally determined values. However, the calculated theoretical FOM does not take into account the change in the physical parameters resulting from the material being operated at an angle from the indicatrix axes (i.e. phase-matched operation). Given the difficult nature of such a measurement, we believe the values given in Table 4.1 to be a reasonable, first-order estimate.

	230 μm	620 μm	930 μm
P_a/L (W/m)	3410	2950	2520
R_t (W/m)	280	250	210

Table 4.1 Thermal loading and estimated thermal-fracture figure-of-merit for $Nd^{3+}:YCa_4O(BO_3)_3$.

4.3 Scaling SFD operation: Prospectives

Optimistically, we can expect that SFD green laser operation with current Nd^{3+} or Yb^{3+} -doped YCOB may achieve power levels of ~ one watt. To obtain the higher powers, thermal design considerations must first be addressed. The use of a slab form with a large aspect ratio would allow the maximum absorbed thermal-power per unit length to be increased by as much as a factor of five, thus allowing for higher pump powers. Efficient edge cooling of the pump face using a bonded composite material,[78] a water cooled sapphire window[79] or copper heat sinking will also give more uniform heat removal and allow the material to be operated closer to the thermal stress FOM. In addition, new orientations of Nd^{3+}:YCOB using phase-matching conditions out of principle planes[36] suggest a factor of two increase in SFD output in the low power case described in section 3.1. When optimized using a controlled cavity mode for efficient conversion of the pump wavelength to the green emission, one could visualize the new phase-matching conditions approaching the one-watt power level.

5. SUMMARY

In this short review, we have described the progress made in the development of the YCOB host material over the last years. As a nonlinear crystal YCOB has several advantages over other nonlinear optical crystals. Nd-doped YCOB shows considerable potential as a practical SFD laser material operating at 530 nm and 666 nm. Yb-doped YCOB offers efficient operation over a broad range of infrared and visible wavelengths and has potential as a medium for femtosecond pulse generation. Scaling of SFD operation has been discussed using a high-brightness multi-diode laser source. Higher

fundamental and SFD laser operation has been achieved. Still higher scaling of SFD operation is possible with the advent of higher-brightness diode-lasers and through optimum configuration of the material's nonlinear and thermal properties.

ACKNOWLEDGEMENTS

The authors acknowledge software and electronic support by Sean Wang of B&W TEK for the high-power pump-source power-supply. They also acknowledge the invaluable technical support of Neil Vanasse for the thermo/mechanical mounting systems. The initial Ti:Sapphire-pumped and low-power diode-pumped experiments were performed also with Jason Eichenholz, Qing Ye, Wong Jang, Lawerence Shah, and Gary Luntz. Absorption and emission spectra were taken with the help of Robert Peale. This work was supported in part by the State of Florida.

REFERENCE

1. S. Nakamura and G. Fasol, *The Blue Laser Diode*, Berlin: Germany: Springer-Verlag, (1997).
2. B. H. T. Chai, Opt. Photon. News, **10**, 31 (1999).
3. F. Mougel, G. Aka, A. Kahn-Harari, H. Hubert, J. M. Benitez, and D. Vivien, Opt. Mater., **8**, 161 (1997).
4. J. M. Eichenholz, D. A. Hammons, L. Shah, Q. Ye, R. E. Peale, M. Richardson, and B. H. T. Chai, Appl. Phys Lett., **74**, 1954 (1999).
5. F. Mougel, F. Augé, G Aka, A. Kahn-Harari, D. Vivien, F. Balembois, P. Georges and A. Brun, Appl. Phys. B, **67**, 533 (1998).
6. Q. Ye, L. Shah, J. Eichenholz, D. Hammons, R. Peale, M. Richardson, A. Chin, and B. H. T. Chai, Opt. Comm., **164**, 33 (1999)
7. D. A. Hammons, J. M. Eichenholz, Q. Ye, B. H. T. Chai, L. Shah, R. E. Peale, M. Richardson, and H. Qiu, Opt. Comm., **156**, 327 (1998).
8. F. Mougel, K. Dardenne, G. Aka, a. Kahn-Harari, and D. Vivien, J. Opt. Soc. Am. B, **16**, 164 (1999).
9. L. F. Johnson and A. A. Ballman, J. Appl. Phys., **40**, 297 (1969).
10. V. G. Dmitriev, E. V. Raevskii, N. M. Rubina, L. N. Rashkovich, O. O. Silichev, and A. A. Romichev, Sov. Tech. Phys. Lett., **5**, 590 (1979).
11. T.Y. Fan, A. Cordova-Plaza, M.J.F. Digonnet, R.L. Byer, and H.J. Shaw, J. Opt. Soc. Am. B **3**, 140 (1986).
12. L. M. Dorozhkin, I. I. Kuratev, N. I. Leonyuk, T. I. Timchneko, A. V. Shestakov, Sov. Tech. Phys. Lett., **7**, 555 (1981).
13. B. S. Lu, J. Wang, H. F. Pan, M. H. Jiang, E. Q. Liu, X. Y. Hou, J. Appl. Phys., **66**, 6052 (1989).
14. J. Bartschke, R. Knappe, K.-J. Boller, and R. Wallenstein, IEEE J. Quantum Electron., **33**, 2295 (1997).
15. D. Jaque, J. Capmany, J. García Solé, Z. D. Luo, and A. D. Jiang, J. Opt. Soc. Am. B, **15**, 1656 (1998).
16. Z. Luo, X. Fang, and Y. Huang, Opt. Comm., **81**, 59 (1991).
17. M. Iwai, Y. Mori, T. Sasaki, S. Nakai, N. Sarukura, Z. Liu, Y. Segawa, Jpn. J. Appl. Phys., **34**, 2338 (1995).
18. I. Schütz, I. Freitag, and R. Wallenstein, Opt. Comm., **77**, 221 (1990).
19. D. Jaque, J. Capmany, F. Molero, and J. García Solé, Appl. Phys. Lett., **73**,. 3659 (1998).
20. D. Jaque, J. Capmany, and J. García Solé, Appl. Phys. Lett., **74**, 1788 (1999).
21. D. Jaque, J. Capmany, and J. García Solé, Appl. Phys. Lett., **75**, 325 (1999).
22. R. C. Powell, *Physics of Solid-State Laser Materials*, New York: USA: Springer-Verlag, (1998).
23. J. Capmany, D. Jaque, J. García Solé, and A. A. Kaminskii, Appl. Phys. Lett., **72**, 531 (1998).
24. A. A. Kaminskii, Quantum. Electron., **28**, 1031 (1998).
25. P. Wang, J. M. Dawes, P. Dekker, D. S. Knowles, J. A. Piper, and B. Lu, "J. Opt. Soc. Am. B, **16**, 63 (1999).
26. E. Montoya, J. Capmany, L. E. Bausá, T. Kellner, A. Diening, and G. Huber, Appl. Phys. Lett., **74**, 3113 (1999).
27. D. A. Hammons L. Shah, J. Eichenholz, Q. Ye, M. Richardson, and B. H. T. Chai, Advanced Solid-State Lasers - OSA Trends in Opt. Photon. Ser., **26**, 286 (1999).
28. Q. Ye and B. H. T. Chai, J. Cryst. Growth., **197**, 228 (1999).
29. S. Lei, Q. Huang, Y. Zheng, A. Jiang and C. Chen, Acta Crystal., **C45**, 1861 (1989).
30. T.N. Khamaganova, V.K. Trunov & B.F. Dzhurinshii, Russian J. Inorg. Chem. **36,** 484 (1991).
31. R. Norrestam, M. Nygen, and J.O. Bovin, Chem. Mater. **4**, 737 (1992).
32. A. B. Ilyuklin and B. F. Dzhurinskii, Russ. J. Inorg. Chem., **38**, 847 (1993).
33. G. Aka, A. Kahn-Harari, d. Vivien, J. –M. Benitez, F. Salin, and J. Godard, Eur. J. Solid State Inorg. Chem., **33**, 727 (1996).
34. M. Iwai, T. Kobayashi, H. Furuya, Y. Mori & T. Sasaki, J. Jnl. Appl. Phys **36**, Pt.2. 276 (1997).

35. W. K. Jang, Q. Ye, D. Hammons, J. Eichenholz, J. Lim, M. Richardson, B. H. T. Chai, and E. W. Van Stryland, IEEE J. Quantum. Electron., **35**, 1826 (1999).
36. H. J. Zhang, X. L. Meng, L. Zhu, C. Q. Wang, R. P. Cheng, W. T. Yu, S. J. Zhang, L. K. Sun, Y. T. Chow, W. L. Zhang, H. Wang, and K. S. Wong, Opt. Comm., **160**, 273 (1999).
37. M. Yoshimura, H. Furuya, T. Kobayashi, K. Murase, Y. Mori, and T. Sasaki, Opt. Lett., **24**, 193 (1999).
38. J. Lu, G. Li, J. Liu, S. Zhang, H. Chen, M. Jiang, and Z. Shao, Opt. Comm., **168**, 405 (1999).
39. F. Augé, F. Balembois, P. Georges, A. Brun, F. Mougel, G. Aka, A. Kahn-Harari, and D. Vivien, Appl. Opt. **38**, 976 (1999).
40. W. Koechner, *Solid-State Laser Engineering*, 3rd ed. Berlin: Germany: Springer-Verlag, (1992).
41. A. N. Pino-Bustamante, Ph. D. dissertation, Univ. of São Paulo, São Paulo, SP, Brasil, (1999).
42. T. M. Pollak, W. F. Wing, R. J. Grasso and E. P. Chicklis, IEEE J. Quantum. Electron., **18**, 159 (1982).
43. V. G. Dmitriev, G. G. Gurzadyan and D. N. Nikogosyan, *Handbook of nonlinear optical crystals*, 2nd ed., Berlin: Germany: Springer-Verlag, (1996).
44. *Crystal guide-Crystals & Materials: Laser Accessories* – CASIX, 21822 Lassen St. #G, Chatsworth, CA 91311, 1998.
45. J. D. Bierlein, H. Vanherzeele, J. Opt. Soc. Am. B, **6**, 622 (1989).
46. B. Henderson and G. F. Imbusch, *Optical Spectroscopy of Inorganic Solids*, New York: USA: Oxford Univ. Press (1989).
47. L. D. DeLoach, S.A. Payne, L.L. Chase, L. K. Smith, W.L. Kway, and W.F. Krupke, IEEE J. Quantum Electron. **29**, 1179 (1993).
48. F. Mougel, G. Aka, F. Salin, D. Pelenc, B. Ferrand, A. Kahn-Harari, and D. Vivien, Advanced Solid-State Lasers - OSA Trends in Opt. Photon. Ser., **26**, 709, 1999.
49. P. Lacovara, H. K. Choi, C. A. Wang, R. L. Aggarwal, and T. Y. Fan, Opt. Lett., **20**, 713 (1991).
50. R. Allen and L. Esterowitz, Electron. Lett., **31**, 639 (1995).
51. C. D. Marshall, L. K. Smith, R. J. Beach, M. A. Emanuel, K. I. Schaffers, J. Skidmore, S. A. Payne, and B. H. T. Chai, IEEE J. Quantum Electron., **32**, 650 (1996).
52. R. Koch, W. A. Clarkson, D. C. Hanna, S. Jiang, M. J. Myers, D. Rhonehouse, S. J. Hamlin, U. Gribner, and H. Schönnagel, Opt. Comm. **134**, 175 (1997).
53. K. Kubodera and J. Noda, Appl. Opt., **21**, 3466 (1982).
54. J. Berger, D. F. Welch, w. Streifer, D. R. Scifres, N. J. Hoffman, J. J. Smith, and D. Radecki, Opt. Lett., **13**, 306 (1988).
55. R. Beach, R. Reichert, W. Benett, B. Freitas, S. Mitchell, a. Velsko, J. Davin, and R. Solarz, Opt. Lett., **18**, 1326 (1993).
56. J. Frauchiger, P. Albers, and H. P. Weber, digest of Topical Meeting on Tunable Solid-State Lasers, paper TuC2 (1989).
57. S. C. Tidwell, J. F. Seamans, M. S. Bowers, and A. K. Cousins, IEEE J. Quantum. Electron., **28**, 997 (1992).
58. T.Y. Fan, A Sanchez, and W. E. DeFeo, Opt. Lett., **14**, 1057 (1989).
59. C. P. Wyss, W. Lüthy, H. P. Weber, L. Brovelli, C. Harder, H. P. Meier, Opt. Quantum Electron., **31**, 173 (1999).
60. D. S. Goodman, W. L. Gordon, R. Jollay, J. W. Roblee, P. Gavrilovic, D. Kuksenkov, A. Goyal, and Q. Zu, SPIE, **3626A**, 1 (1999).
61. D. Wright, P. Greve, J. Fleischer and L. Austin, Opt. Quantum Electron., **24**, S993 (1992).
62. T. Baer, J. Opt. Soc. Am. B, **3**, 1175 (1986).
63. T. J. Kane, IEEE Photon. Tech. Lett., **2**, 244 (1990).
64. T. J. Kane, Short Course Notes, Conf. Laser Electro. Opt. (1997).
65. H. Hemmati, IEEE J. Quantum Electron., **28**, 1169 (1992).
66. M. Oka and S. Kubota, Opt. Lett., **13**, 805 (1988).
67. J. L. Nightingale and J. K. Johnson, U.S. Patent 5 052 815 (1992).
68. W. L. Nighan, J. Cole, and T. M. Baer, U.S. Patent 5 446 749 (1995).
69. L. R. Marshall, U.S. Patent 5 511 085 (1996).
70. T. Y. Fan and A. Sanchez, IEEE J. Quantum. Electron., **26**, 311 (1990).
71. T. Y. Fan and R. L. Byer, IEEE J. Quantum. Electron., **23**, 605 (1987).
72. W. P. Risk, J. Opt. Soc. Am. B, **5**, 1412 (1988).
73. P. Laporta and M.Brussard, IEEE J. Quantum. Electron., **27**, 2319 (1991).
74. F. Sanchez, M. Brunel, and K. Aït-Ameur, J. Opt. Soc. Am. B, **15**, 2390 (1998).
75. J. M. Eggleston, T. J. Kane, K. Kuhn, J. Unternahrer and R. L. Byer, IEEE J. Quantum Electron., **20**, 289 (1984).
76. D. S. Sumida and B. A. Wechsler, Short Course Notes, Conf. Laser Electro. Opt. (1997).
77. W. F. Krupke, M. D. Shinn, J. E. Marion, J. A. Caird, and S. E. Stokowski, J. Opt. Soc. Am. B, **3**, 102 (1986).
78. M. Tsunekane, N. Taguchi, T. Kasamatsu, and H. Inaba, IEEE J. Sel. Top. Quantum Electron., **3**, 9 (1997)
79. R. Weber, B. Neuenschwander, M. MacDonald, M. B. Roos, and H. P Weber, IEEE J. Quantum. Electron., **34**, 1046 (1998)